Directional Fano Resonance in a Silicon Nanosphere Dimer

Jiahao Yan, Pu Liu, Zhaoyong Lin, Hao Wang, Huanjun Chen, Chengxin Wang, and Guowei Yang*

State Key Laboratory of Optoelectronic Materials and Technologies, Institute of Optoelectronic and Functional Composite Materials, Nanotechnology Research Center, School of Physics & Engineering, Sun Yat-sen University, Guangzhou 510275, Guangdong, PR China

ABSTRACT Fano resonance arising from the interaction between a broad "bright" mode and a narrow "dark" mode has been widely investigated in symmetry-breaking structures made of noble metals such as plasmonic asymmetric oligomers or other well-designed nanostructures. However, Fano resonance in nanoscale all-dielectric dimers has not been experimentally demonstrated so far. We report the first experimental observation of directional Fano resonance in silicon nanosphere dimers (both homodimer and heterodimer) and clarify that the coupling between magnetic and electric dipole modes can easily generate Fano resonance in all-dielectric oligomers, distinctly differing from conventional Fano resonances based on electric responses or artificial optical magnetism. A silicon nanosphere dimer, exhibiting a strong magnetic response inside and an electric enhancement in the gap, is an excellent structure to support magnetic-based Fano scattering. Interactions between magnetic and electric dipoles can suppress backward scattering and enhance forward scattering at Fano wavelengths. This directional scattering is much more prominent than that from a single silicon sphere and shows promising applications in areas such as directional nanoantenna or optical switching, opening up avenues for developing all-dielectric low-loss metamaterials or nanophotonic devices at visible wavelengths.

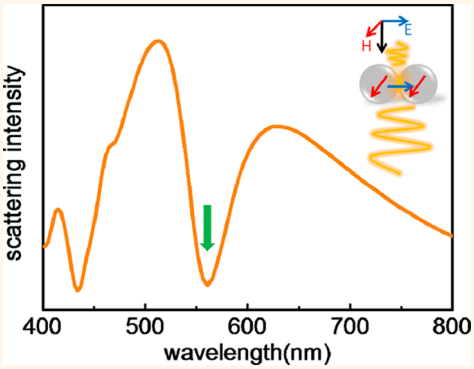

KEYWORDS: silicon sphere dimer · all-dielectric · Fano resonace · directional scattering · magnetic response

Fano resonance, which is distinguished by an asymmetric line shape or a narrow resonance dip,[1−5] can be generated from the destructive interference between an overlapping broad resonance with a narrow resonance. This unique line shape, which is sensitive to geometry or local environment,[2] has great potential in applications such as plasmonic sensing,[6,7] chemical or biological sensing,[8] and optical antenna or switching.[9,10] Conventional Fano resonances in metallic particle oligomers[5,11−13] or other plasmonic nanostructures[14−16] have been widely investigated. In particular, Fano resonances can be observed in heterodimers such as nanorod dimers with different aspect ratios[17,18] or nanoparticle dimers with different radii or different materials.[19,20] Because of symmetry breaking, heterodimers exhibit more complex coupling behaviors and give rise to Fano resonance. Very recently, all-dielectric nanostructures exhibiting low-loss scattering and strong magnetic response at visible wavelengths have drawn increasing attention.[21,22] Although there is some research on Fano resonance based on dielectric materials, such as photonic crystals with continuum Mie scattering and a narrow Bragg band,[23] microscale dielectric bispheres with whispering gallery modes[24] or all-dielectric antennae operating in the microwave region combined with a dipole source,[25] there have been so far no reports on Fano resonance in all-dielectric nanosphere dimers at visible wavelengths. We note that Fano resonances observed in all-dielectric trimers and heptamers[21,22,26] arise from detached silicon nanodisks fabricated *via* electron-beam lithography and have no directional feature. Therefore, the generation of Fano resonance in self-assembled and nearly touching silicon nanosphere oligomers still remains unclear.

Herein, we demonstrate experimentally for the first time that the directional Fano resonance can easily arise in a silicon nanosphere dimer and propose a new physical origin of the Fano-type backward scattering in all-dielectric nanosphere oligomers. Compared with plasmonic oligomers, Fano resonance in silicon nanosphere dimers has

* Address correspondence to stsygw@mail.sysu.edu.cn.

Received for review December 15, 2014 and accepted February 15, 2015.

Published online February 15, 2015
10.1021/nn507148z

© 2015 American Chemical Society

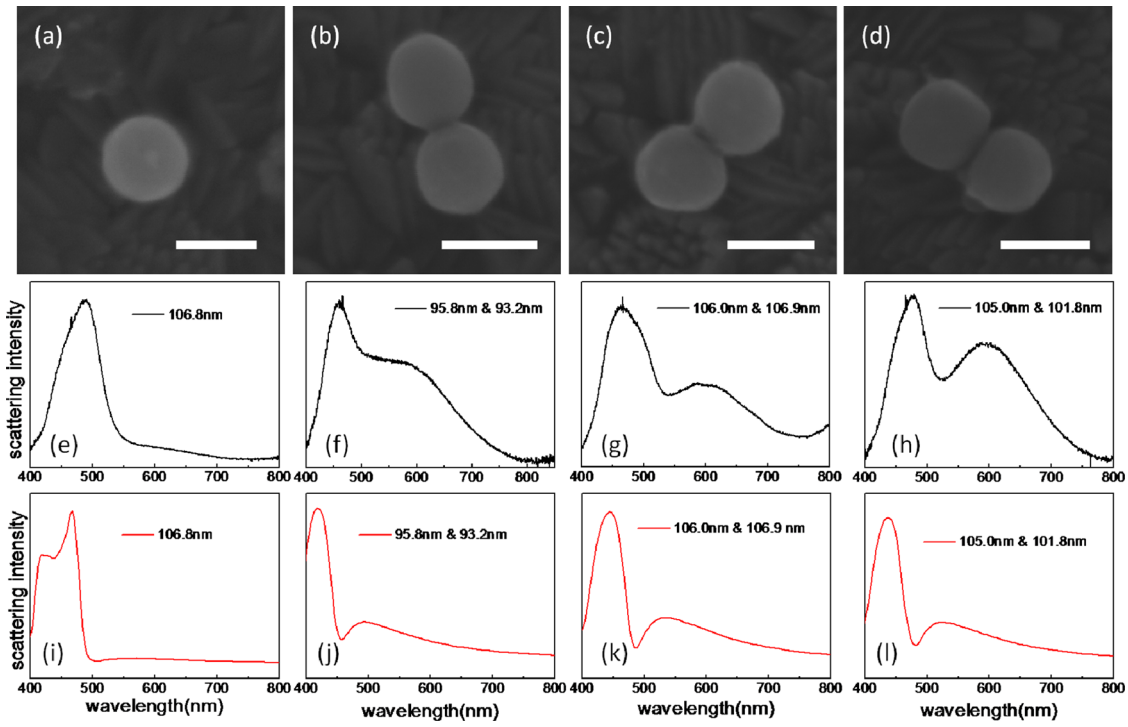

Figure 1. Backward scattering properties of single silicon sphere and silicon nanosphere homodimers. (a) The SEM image of single silicon sphere with diameter of 106.8 nm. (b–d) The SEM images of three "homodimers": 95.8 and 93.2 nm dimer (b); 106.0 and 106.9 nm dimer (c); 105.0 and 101.8 nm dimer (d). And the scale bar in all SEM images is 100 nm. The corresponding experimental scattering spectra (e–h) and simulated scattering spectra (i–l) for the nanostructures (a–d).

some unique advantages. First, dielectric nanospheres like silicon with sizes from 80 to 200 nm have strong magnetic dipole resonances in the visible range.[27–29] Considering that optical magnetism is of critical importance in achieving negative refraction in metamaterials,[30] the magnetic-based Fano resonance is significant for applications in the unit cells of metamaterials. Although the Fano resonances have been investigated in some "artificial magnetic" structures,[3,4] silicon nanospheres with intrinsic magnetic response may be a better choice. Second, when two silicon nanospheres are in close proximity, the two magnetic dipoles couple to produce a narrow coupled magnetic response while the two electric dipoles couple to produce a broad electric response with strong electric enhancement in the gap between the two spheres. Unlike the plasmonic dimer that has strong absorption, the field enhancement in silicon-dimer gap almost radiates.[31] Hence the broad "bright" electric mode in the silicon dimer interacting with the narrow "dark" magnetic mode in the far field generates a Fano resonance. Finally, Fano resonance caused by interacting electric and magnetic dipole resonances has directional selectivity.[32–34] A narrow Fano resonance dip can be seen in the backward scattering, whereas enhanced radiation is observed in the forward scattering from a silicon dimer. The difference between forward and backward scattering for a single nanosphere is unnoticeable[29] because the electric and magnetic dipole responses in a single nanosphere are narrow and detached in the spectra. Fortunately, the formation of a dimer overcomes this disadvantage and generates an obvious unidirectional scattering. Therefore, these novel properties enable silicon nanosphere dimers to become a superior magnetic-based Fano resonance device in nanophotonics applications. For instance, it can work as a directional optical antenna.[10,35] Considering that the scattering is sensitive to polarization, the silicon dimer can also act as a polarization-dependent optical switch.

RESULTS AND DISCUSSION

Silicon nanospheres with diameters from 80 to 200 nm were fabricated by femtosecond laser ablation in liquid (fs-LAL). We used an ultrafast laser with a pulse duration of 35 fs, and single-pulse energy of 4 mJ. After laser ablating, we produced a silicon colloid suspended in solution. We then transferred one drop of the solution to a piece of indium–tin–oxide (ITO) glass. During evaporation, big droplets would divide into small droplets that contain less silicon spheres. When the droplets dried up, multiple silicon spheres self-assembled as dimers, trimers or other oligomers *via* capillary forces.

We studied the Fano effect in homodimers first. Typical homodimers are shown in Figure 1b–d; a single silicon sphere is presented in Figure 1a for comparison. Sizes of each homodimers were measured from scanning electron microscope (SEM) images employing multimeasurement averaging; if the size

difference between the two spheres is less than 4 nm, we identify them as "homodimers". Figure 1e–h shows the backward scattering spectra measured by a dark-field optical microscope integrated with a quartz-tungsten-halogen lamp, a monochromator, and a charge-coupled device (CCD) camera. The scattering spectrum of a single silicon sphere of diameter 106.8 nm shows a dominant magnetic dipole peak near $\lambda = 500$ nm. However, when two nanospheres are in proximity, the scattering spectrum changes dramatically and reveals a Fano line shape. When two silicon spheres in a dimer have similar diameters ($d = 95.8$ and 93.2 nm in Figure 1b), a Fano asymmetric line shape around 500 nm can be seen (Figure 1f). Compared with a single silicon nanosphere, the scattering intensity in the longer wavelength region is strongly enhanced in a dimer, because the electric field enhancement occurs in the gap between the two nanospheres. Hence, a narrow magnetic dipole resonance inside the silicon spheres interferes destructively with the broad electric resonance in the gap, and as a result, the magnetic resonance creates a Fano dip in the backward scattering spectrum. In larger silicon dimers, this effect is more obvious as seen in Figure 1g ($d = 106.0$ and 106.9 nm) and h ($d = 105.0$ and 101.8 nm). More distinct Fano dips can be seen between two peaks, because the magnetic response is stronger and the interaction is more effective with increasing size. To confirm the phenomenon observed in the experiment, we performed numerical simulations using the finite-difference time-domain (FDTD) method. The dimer nanostructures were illuminated by normal incident plane-waves in the visible spectral range ($\lambda = 300–900$ nm) polarized along the dimer axis. The dielectric function of silicon was obtained from Palik.[36] Silicon spheres were selected vaccording to diameter using measurements obtained from SEM images; the distance between two spheres was set to 0 nm. To be in accord with the experiments, a 2 nm-thick silica layer was specified in all simulation results. As will be shown below, the ITO glass substrate has little effect on the backward scattering spectra, so we calculated the spectra assuming a free space and ignoring the substrate. The simulation results, presented in Figure 1i–l, well match the experiment results. Small discrepancies occur mainly because of a slight difference in magnetic response between the two because of defects in the fabricated silicon spheres, and because there is a difference in the electric field distributions in gap caused by imperfect circular shapes.

When the diameters of the two silicon spheres in a dimer are different, the spectra clearly changes. Three types of heterodimers are presented in Figure 2a–c. The resonant wavelength and intensity of the magnetic response in the silicon sphere is sensitive to size. According to Mie theory,[27] the magnetic resonance peak is red-shifted on increasing the size of the silicon sphere. Thus, the dimer with $d = 100.0$ nm and $d = 126.6$ nm has different magnetic resonance peaks, and they both interact with the electric resonance in the gap. Two narrow Fano dips can be distinguished at $\lambda = 492$ nm and $\lambda = 591$ nm (Figure 2d). For the dimer with $d = 114.5$ and 134.5 nm (Figure 2e), the Fano effect happens at $\lambda = 500$ nm and $d = 595$ nm. Similarly, two dips can be observed in Figure 2f at $\lambda = 511$ and 592 nm caused by spheres with $d = 115.2$ and 129.8 nm, respectively. The simulation results are presented in Figure 2g–i. Two Fano dips can also be seen in the simulation results; the small discrepancies in the peak and dip positions are caused by imperfections in the circular spheres (see ref 29 for a discussion). Of note is that the scattering intensity exhibits a slight difference between experiment and simulation below the 500 nm wavelength region, because silicon spheres fabricated by laser ablation have relative weaker electric dipole resonance compared with simulation results based on parameter values of Palik; this will be discussed later. The quantum efficiency of our CCD near the ultraviolet range drops quickly; thus the vmeasured scattering intensities decrease to nearly zero at $\lambda = 400$ nm. For a silicon sphere of size 90 to 150 nm, the magnetic quadrupole and the electric quadrupole resonances often arise below $\lambda = 400$ nm and are very weak[28] being distance from the Fano dips (magnetic dipole resonances). Therefore, we can ignore them and focus entirely on the coupling mechanism between the magnetic and electric dipole resonances.

Fano resonance in silicon nanosphere dimers is unique, because the electric dipole radiation generated in the gap is a natural broad-resonance mode, which can be generated easily and remain unchanged when changing the size of silicon spheres. At the same time, the magnetic dipole radiation in the silicon sphere has a natural narrow line shape and the resonant wavelength remains unchanged when the sphere is combined with the dimer. For these two reasons, Fano resonance is much easier to generate in silicon dimers. When changing the diameter of the silicon spheres, we can tune the Fano resonance to any specified wavelength. From homodimer to heterodimer, the number of Fano resonance dips changes from single to double.

To understand the coupling mechanism better, a theoretical calculation was performed using Mie theory and the analytical dipole–dipole model.[31] Investigating the splitting of degenerate modes and the switching of dark modes in symmetry breaking systems has been widely used to study the coupling mechanism,[37,38] but in our system, the main mechanism is hybridization[39] between the dipole modes, so it is sufficient to study the dipole–dipole interaction. First, we study the scattering properties of a single silicon nanosphere. Scattering cross sections for a

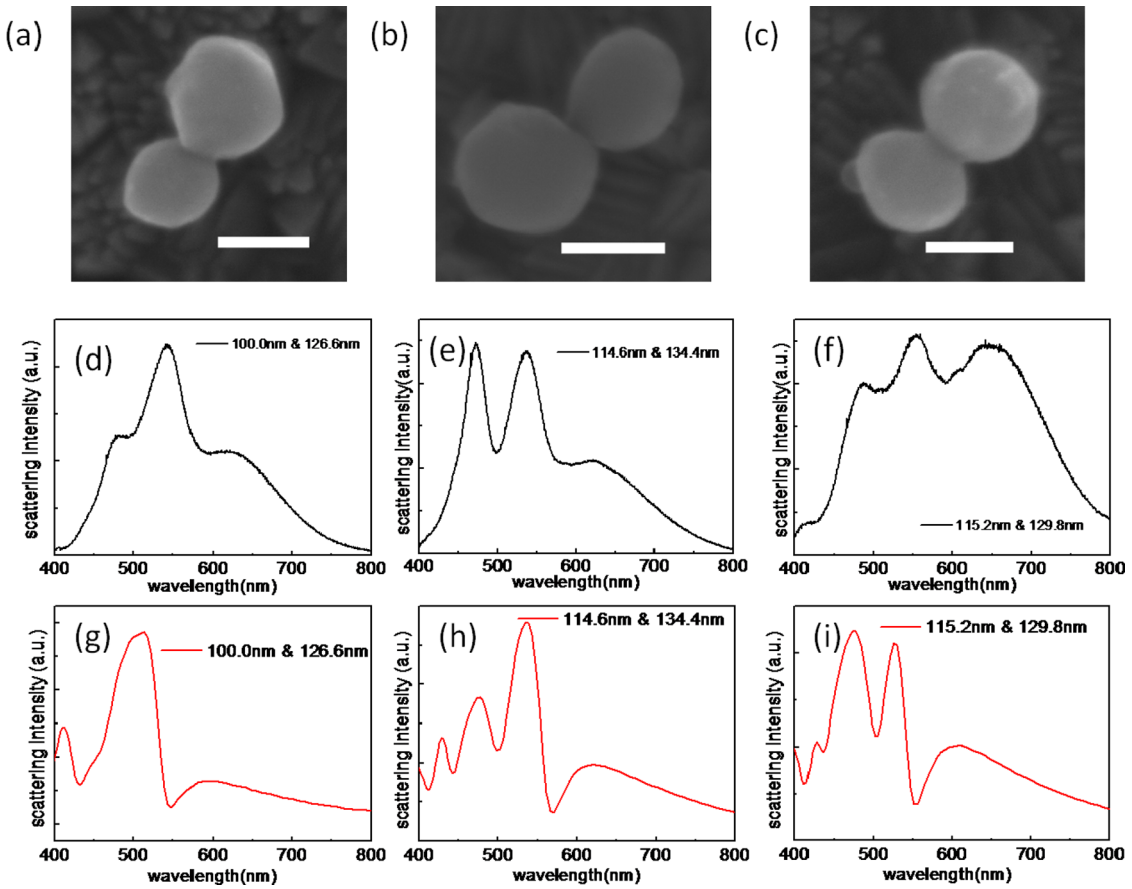

Figure 2. Backward scattering properties of silicon nanosphere heterodimers. (a–c) The SEM images of three typical heterodimers: 100.0 and 126.6 nm dimer (a); 114.5 and 134.4 nm dimer (b); 115.2 and 129.8 nm dimer (c). And the scale bar in all SEM images is 100 nm. (d–f) The corresponding experimental scattering spectra, and two Fano resonance dips can be seen. (g–i) Simulated scattering spectra for the nanostructures (a–c).

sphere can be decomposed into a series of multipolar contributions,[40]

$$\sigma_{scat} = \frac{2\pi}{k^2}\sum_{n=1}^{\infty}(2n+1)(|a_n|^2+|b_n|^2) \quad (1)$$

where k is the wave vector, and a_n and b_n are the electric and magnetic Mie coefficients. For nanospheres with sizes much smaller than the incident wavelength, only the first two coefficients dominate, so the scattering cross-section of a silicon sphere with d = 130 nm can be describe by a_1 and b_1 being proportional to the electric and magnetic dipoles. The scattering spectra contributed by a_1 and b_1 (Figure 3a) show two well-defined resonance peaks at 460 nm (electric dipole) and 550 nm (magnetic dipole), and the interference between the electric and magnetic dipoles leads to directional scattering (Figure 3b). However, the electric and magnetic modes in a single sphere are narrow and detached in the spectrum, so the unidirectional scattering is not quite obvious, not to mention the directional Fano resonance.

To generate directional Fano resonance, one needs a broad electric mode combined with a narrow magnetic mode, or vice versa. On the basis of this motivation, we tried to engineer the electric and magnetic dipole resonances by combining a single sphere with a dimer. According to the dipole–dipole model,[31] each induced dipole in the spheres experiences an incident field and the dipole–dipole interaction with the induced dipole from the other sphere. Induced magnetic dipoles m_{1x} and m_{2x}, induced electric dipoles p_{1y} and p_{2y} are produced under y-axis polarization along the dimer axis (Figure 3e). The induced dipole can be expressed as

$$p_{1y} = \varepsilon_0\varepsilon_h\alpha_e E_0 + \alpha_e k^2 g_{yy} p_{2y} \quad (2)$$

$$p_{2y} = \varepsilon_0\varepsilon_h\alpha_e E_0 + \alpha_e k^2 g_{yy} p_{1y} \quad (3)$$

$$m_{1x} = -\frac{\alpha_m}{Z}E_0 - \alpha_m k^2 g_{xx} m_{2x} \quad (4)$$

$$m_{2x} = -\frac{\alpha_m}{Z}E_0 - \alpha_m k^2 g_{xx} m_{1x} \quad (5)$$

where ε_0 and ε_h are the vacuum and relative permittivities, $Z = (\mu_0\mu_h/(\varepsilon_0\varepsilon_h))^{1/2}$ is the vacuum impedance, k the wavenumber, E_0 the incident electric field, g_{xx} and g_{yy} are scalar Green's functions related to the distance between two spheres, $\alpha_e = (6\pi i/k^3)a_1$ and

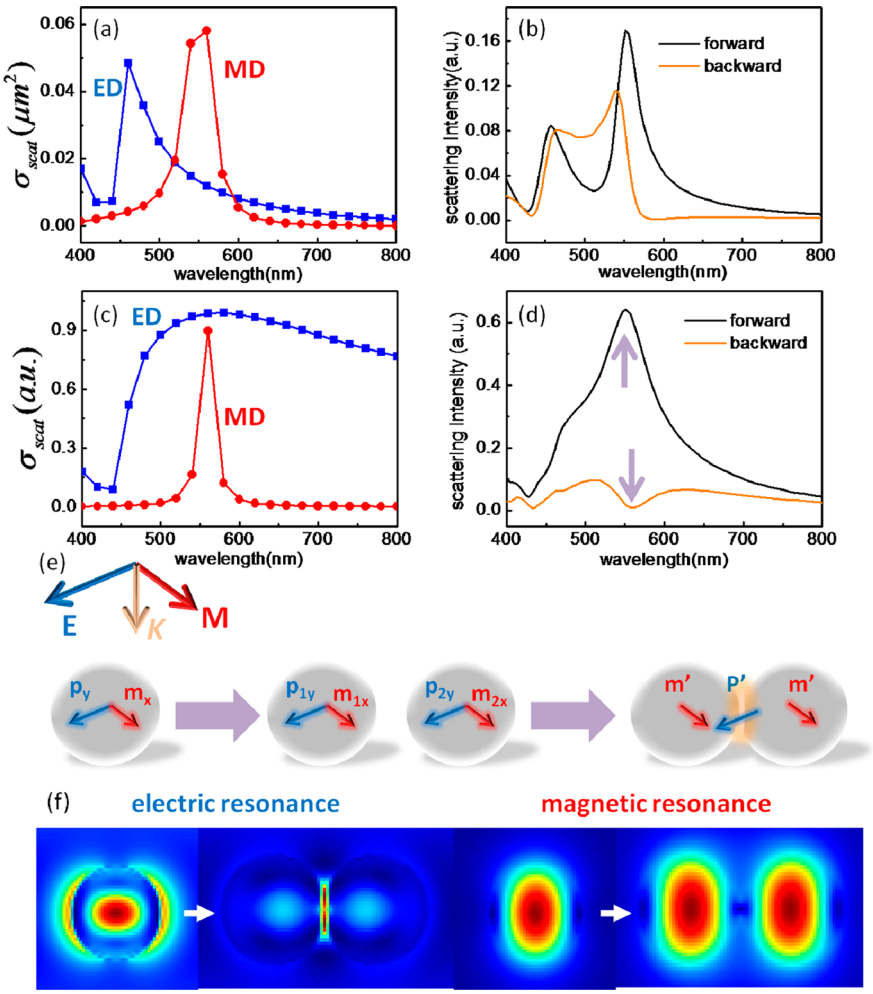

Figure 3. A physical model for the generation of Fano resonance and unidirectional scattering. (a) Contributions of electric dipole (blue curve) and magnetic dipole (red curve) to the scattering cross section in a silicon nanosphere with the diameter of 130 nm. (b) The simulated forward (black curve) and backward scattering (orange curve) spectra of a silicon nanosphere with the diameter of 130 nm. (c) The scattering cross section contributed by electric gap mode (blue curve) and hybrid magnetic dipole mode (red curve) in nearly touched homodimer. (d) The simulated forward (black curve) and backward scattering (orange curve) spectra of a silicon homodimer with diameters of 130 nm. (e) The process diagram on how the electric dipole and magnetic dipole change when combined to dimer. The dimer is excited by a plane wave polarizing along the dimer axis from top. (f) The simulated electric field distributions of single sphere and silicon dimer at the resonant wavelength (left) and simulated magnetic field distributions of single sphere and silicon dimer (right).

$\alpha_m = (6\pi i/k^3)b_1$ are the electric and magnetic polarizabilities of a single sphere, which are related to Mie coefficients a_1 and b_1. To simplify the analysis, one can define equivalent polarizabilities,

$$\tilde{\alpha}_{ey} = \frac{\alpha_e}{1 - \alpha_e k^2 g_{yy}} \quad (6)$$

$$\tilde{\alpha}_{mx} = \frac{\alpha_m}{1 + \alpha_m k^2 g_{xx}} \quad (7)$$

The induced dipoles then can be rewritten as

$$p_{1y} = p_{2y} = \varepsilon_0 \varepsilon_h \tilde{\alpha}_{ey} E_0 \quad (8)$$

$$m_{1x} = m_{2x} = -\frac{\tilde{\alpha}_{mx}}{Z} E_0 \quad (9)$$

which are similar to the expressions in a single sphere. Hence we can use the equivalent polarizabilities $\tilde{\alpha}_{ey}$ and $\tilde{\alpha}_{mx}$ to represent the new electric gap and hybrid magnetic dipole modes. Putting $\tilde{\alpha}_{ey}$ and $\tilde{\alpha}_{mx}$ in eq 1, the scattering cross-section of a 130 nm homodimer contributed by each coefficient can be calculated (Figure 3c) and well verifies the coupling mechanism described above. The variations in the electric and magnetic dipoles are presented in Figure S1 (Supporting Information). When single spheres combine with a dimer, the electric dipole resonances in each sphere hybridizes strongly and produce a new electric dipole mode in the gap that is broad and bright. The electric field distributions calculated by the FDTD method (Figure 3f) illustrate this process well. For a single sphere, the electric field distribution shows a dipolar electric field feature around the sphere. Nevertheless, when two spheres are brought together, an enhanced electric field can be seen

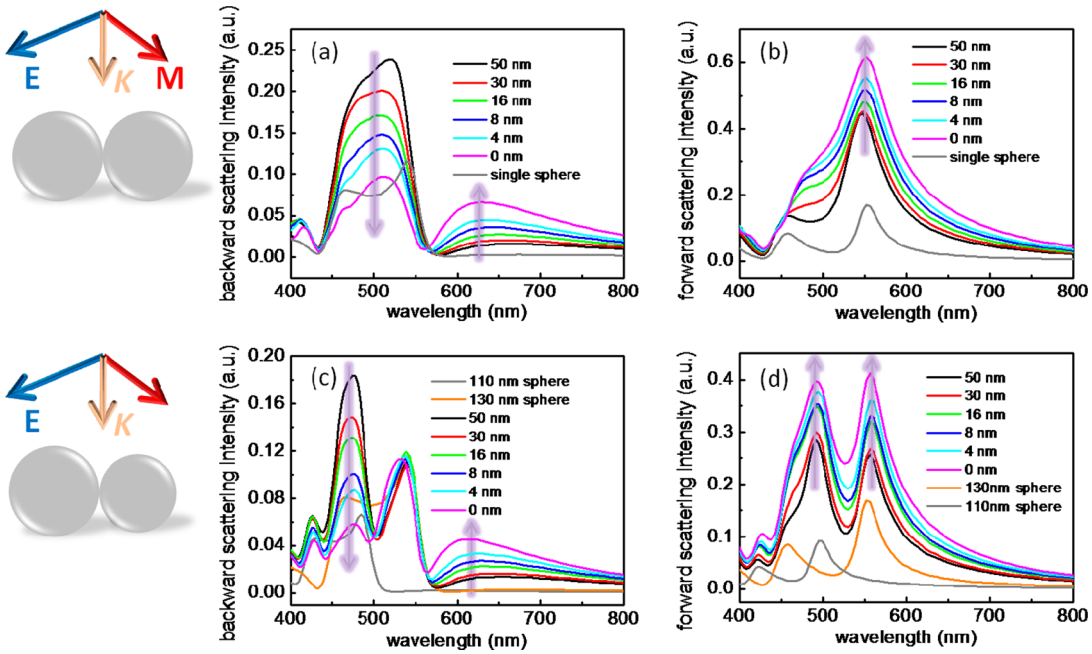

Figure 4. Calculated scattering properties of the silicon nanosphere homodimer and heterodimer with different gap distance. (a) Backward scattering spectra of a homodimer with the sphere diameters of 130 nm. Purple arrows reveal the spectral variation when reducing the gap distance from 50 to 0 nm. (b) Forward scattering spectra of a homodimer with the sphere diameters of 130 nm. Purple arrow reveals the spectral variation when reducing the gap distance from 50 to 0 nm. Gray curves plotted in (a) and (b) show the scattering property of single 130 nm sphere as a comparison. (c) Backward scattering spectra of a heterodimer with the sphere diameters of 110 and 130 nm. (d) Forward scattering spectra of a heterodimer with the sphere diameters of 110 and 130 nm. Orange and gray curves in (c) and (d) represent the scattering from single 130 and 110 nm spheres, respectively.

localized in the gap. Meanwhile, the magnetic dipole resonance can also hybridize with each other (Figure 3f). Although the magnetic field distribution stays nearly unchanged when combined with the dimer, the parallel and side-by-side magnetic dipoles will reduce the dipole moment and narrow the magnetic resonance peak. Consequently, a much broader electric dipole mode and a narrower magnetic dipole mode develop in the dimer structures (Figure 3c).

The mechanism behind directional scattering can be further understood by calculating the far-field scattering intensity distribution[32−34,41]

$$I(\theta, \varphi) \propto \frac{[\sin^2 \varphi(\tilde{\alpha}_{ey}+\tilde{\alpha}_{mx} \cos \theta)^2+ \cos^2 \varphi(\tilde{\alpha}_{ey} \cos \theta+\tilde{\alpha}_{mx})^2]}{k^2} \quad (10)$$

where θ is the scattering angle and φ the angle vbetween the incident field and the scattering plane. For forward scattering, $\theta = 0°$; for backward scattering, $\theta = 180°$. Hence the changes in $\tilde{\alpha}_{ey}$ and $\tilde{\alpha}_{mx}$ as a function of wavelength determine the unidirectional scattering properties. At the Fano resonant wavelength (λ = 550 nm), the hybrid magnetic dipole resonance reaches maximum and has a near-equal dipole moment as that for the electric gap mode. As a result, a distinct Fano dip arises in the backward direction ($\cos \theta = -1$) whereas in forward scattering ($\cos \theta = 1$) it is clearly enhanced. The simulated spectra for the homodimer with diameter 130 nm (Figure 3d) reveal this unique directional Fano resonance, and the forward scattering intensity is almost 64 times larger than that for backward scattering at λ = 550 nm.

As discussed above, the hybrid magnetic mode is relatively stable, but the electric gap mode distributed on the surface is sensitive to surroundings and influences the Fano effect markedly. Hence, it is necessary to study the effect of gap mode in detail. We choose a typical homodimer with two 130 nm-diameter spheres and a typical heterodimer with 130 and 110 nm diameter spheres as examples to reveal the influence of different gap distance. For the homodimer, when the gap distance is large (50 nm), the backward scattering spectrum (black curve in Figure 4a) appears as a simple superposition from the scattering of two individual sphere (gray curve in Figure 4a). The same phenomenon can be seen in the forward direction (Figure 4b). Nevertheless, on decreasing the gap distance, the coupling effect and directional scattering becomes increasingly more obvious. The backward scattering intensity within the longer wavelength range of around λ = 650 nm is enhanced (Figure 4a) because the broad electric gap mode becomes stronger, whereas the backward scattering is suppressed gradually around λ = 500 nm for the enhanced electromagnetic interaction (Figure 4a). In contrast, in the forward direction, the scattering intensities around λ = 500 nm increase gradually when changing the gap distance from 50 to 0 nm in consequence of the coupling

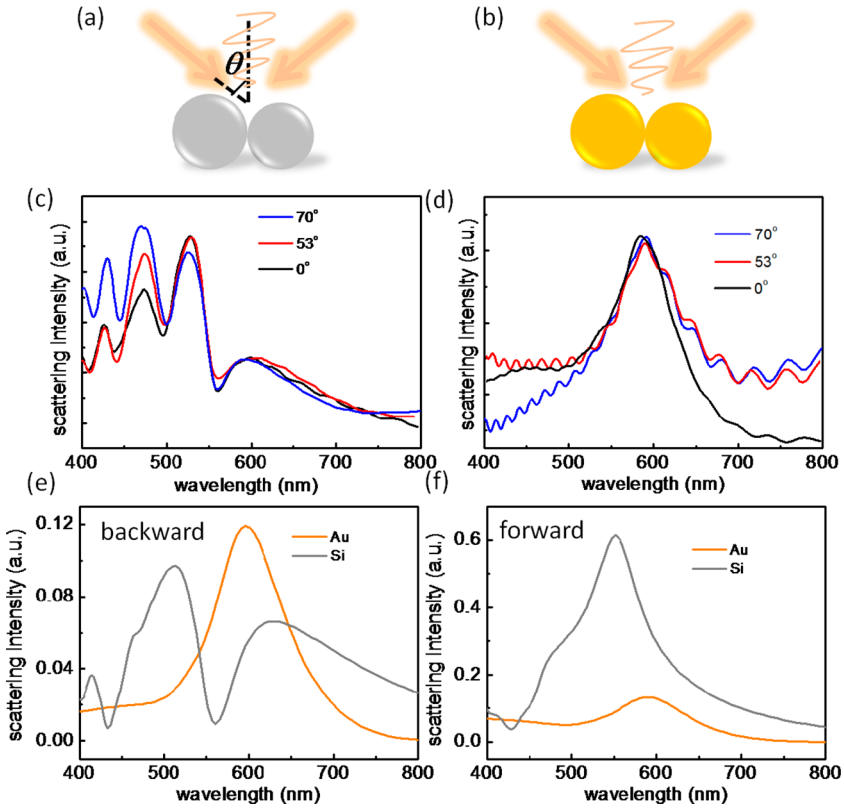

Figure 5. Comparison between silicon nanosphere and gold nanosphere dimers as a nanoantenna. (a,b) Schematics showing how to excite and collect the scattered light in experiment. θ is the incident angle. (c) The collected backward scattering from silicon heterodimer with d = 130 and 110 nm varied with incident angle. (d) The collected backward scattering from gold heterodimer with d = 130 and 110 nm varied with incident angle. (e) Calculated backward scattering spectra of silicon (gray curve) and gold (orange curve) homodimers with d = 130 nm. (f) Calculated forward scattering spectra of silicon (gray) and gold (orange curve) homodimers with d = 130 nm.

between the electric-gap and hybrid-magnetic modes (Figure 4b). This demonstrates that a nearly touching silicon dimer is the best choice to generate a prominent Fano resonance and unidirectional scattering. For heterodimer, the directional scattering is a little bit complex (Figure 4c and d). The scattering spectra of single 130 and 110 nm spheres are also provided (orange and gray lines) to help understand the coupling mechanism better. Two silicon spheres of different sizes interact with the electric gap mode and generate two Fano dips in the backward spectra. When decreasing the gap distance, the scattering intensities around λ = 610 nm are enhanced and the intensities around λ = 485 nm are reduced gradually (Figure 4c) because of the enhanced gap mode and electromagnetic interaction. Similarly, when decreasing the gap distance, two enhanced resonance peaks can be obtained in the forward direction where Fano dips happen in the backward direction (Figure 4d).

Perhaps the greatest difference between a dielectric nanoantenna and a plasmonic nanoantenna is their directional scattering. How the angle of incoming light influences the scattering spectra would provide good insight into the difference between dielectrics and metals. In the experiments, the nanosphere dimer was illuminated *via* a dark-field objective with an incidence angle of 53°, and the scattered light was collected over the sample by the same objective lens (Figure 5a and b). Because of its directional scattering feature, the incidence angle has some effects on the scattering spectra of the silicon nanosphere dimer (Figure 5c). When increasing the incidence angle θ, the scattering signals collected by dark-field objective are no longer pure backward scattered light and more like the light scattered off to the side, which contains both forward and backward components. For large incidence angle (blue curve in Figure 5c), the suppression of scattering intensities becomes obscured and the scattering peak at λ = 485 nm becomes stronger. The influence of incidence angle can explain the discrepancy between experiment and simulation in the heterodimer (Figure 5d–h). The relative strong scattering peak below λ = 500 nm arises from the 53° incidence angle in the experiment. In contrast, the incidence angle has little influence on the scattering behavior of the gold heterodimer. In Figure 5d, the nearly touching gold dimer exhibits a plasmon resonance peak near 600 nm based on plasmon hybridization.[39] Because this hybridization couples the two electric dipole modes, the directional Fano resonance cannot be created. Moreover, to verify low intrinsic losses in the silicon sphere, the scattering cross

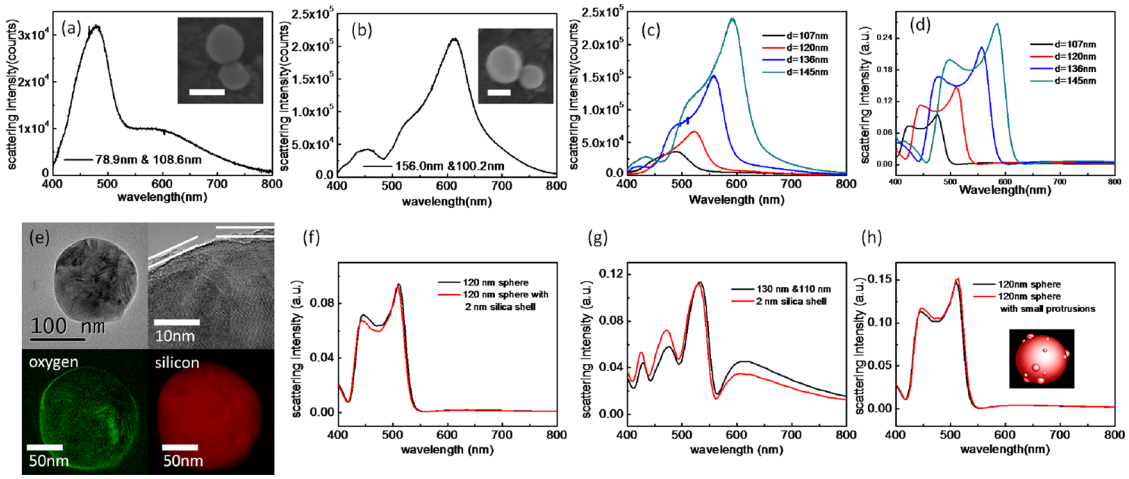

Figure 6. Influences of particle size and surface morphology on scattering property. (a) The backward scattering of a quite small sphere (78.9 nm) combining with a 108.6 nm sphere. Inset is the SEM image of this dimer, and the scale bar is 100 nm. (b) The backward scattering of a fairly big sphere (156.0 nm) combining with a 100.2 nm sphere. Inset is the SEM image of this dimer, and the scale bar is 100 nm. (c) The measured backward scattering spectra of single silicon spheres with different sizes. (d) Calculated scattering spectra of single spheres with different sizes. (e) TEM image of a typical silicon nanosphere with the diameter more than 100 nm (upper left). High resolution TEM image of the silicon sphere. The regions confined by white lines indicates the thin amorphous oxide layer (upper right). The elements mapping of oxygen and silicon (bottom). (f) The backward scattering from a 120 nm sphere with 2 nm silica shell compared with a pure 120 nm silicon sphere. (g) The backward scattering from silicon heterodimer with 2 nm silica shells (red curve) and the backward scattering from heterodimer without silica shell (black curve). (h) Backward scattering of 120 nm single sphere with small protrusions (red line) and smooth sphere (black line).

sections were calculated and compared with that of a Au nanosphere in Figure S2 (Supporting Information). A silicon nanosphere of diameter 130 nm has a larger scattering cross-section over a relatively broad spectral range (450−560 nm) especially at the strong magnetic resonant wavelength. When combined with a dimer, although the scattering intensity in the backward direction is comparable (Figure 5e), the forward scattering of the silicon dimers are much stronger than the scattering intensity from a gold dimer (Figure 5f). Hence, we believe the silicon nanosphere dimer will be a more efficient scatterer with unidirectional features than a plasmonic one.

Next, we investigated how sphere size and material properties influence the Fano resonance (Figure 6). Not all heterodimers can generate two Fano dips, and it depends on sphere sizes. In the experiments, two extreme cases were studied (Figure 6a and b). For the dimer with d = 78.9 and 108.6 nm, the magnetic response in the smaller-diameter sphere is much weaker compared with the electric gap mode, so the dominating mechanism is the interaction between the magnetic response in the larger sphere and the electric gap mode. Thus, only one Fano dip can be seen at λ = 530 nm (Figure 6a). However, the dimer with d = 156.0 and 100.2 nm produces differences. Although the smaller sphere is able to generate a proper magnetic response with an electric gap mode coupling, the magnetic response in the larger sphere is so strong that it dominates any influence of the gap mode. Hence, the spectrum in Figure 6b presents a single-sphere scattering line shape. The single-sphere scattering spectra in Figure 6c support this discussion above. When increasing the sphere size, the magnetic resonance is red-shifted and enhanced. Therefore, the magnetic dipole resonance of the 78.9 nm sphere (Figure 6a) is quite weak and close to the ultraviolet region, and this is why the 108.6 nm sphere dominates. From Figure 6c, the difference in intensity between the 145 and 107 nm spheres is quite large, so it is easily concluded that the 156.0 nm sphere dominates (Figure 6b). The simulation results of single spheres are presented in Figure 6d. Comparing experimental and simulation results, the total lineshapes and the location of the magnetic resonant peaks are consistent implying that parameter values of Palik can be used to simulate our experiment well. One difference is that the electric dipole peaks in the measured spectra are weaker than in simulated spectra, and that is why a discrepancy exists at smaller wavelength region between simulated and measured spectra in Figures 1 and 2. The electric dipole mode in the silicon sphere is partially distributed on the surface (Figure 3f) and is sensitive to morphology and surroundings; hence the slight discrepancy between experimental and simulation results is inevitable. Figure 6e gives the transmission electron microscope (TEM) images of a large silicon sphere (>100 nm) fabricated by fs-LAL. The high-resolution TEM and the elemental mapping images reveal that the polycrystalline silicon sphere is coated with a very thin (1−2 nm) amorphous oxide layer, so the oxide layer has little influence on size measurement and scattering properties (Figure 6f and g). The presence of the oxide layer weakens the electric

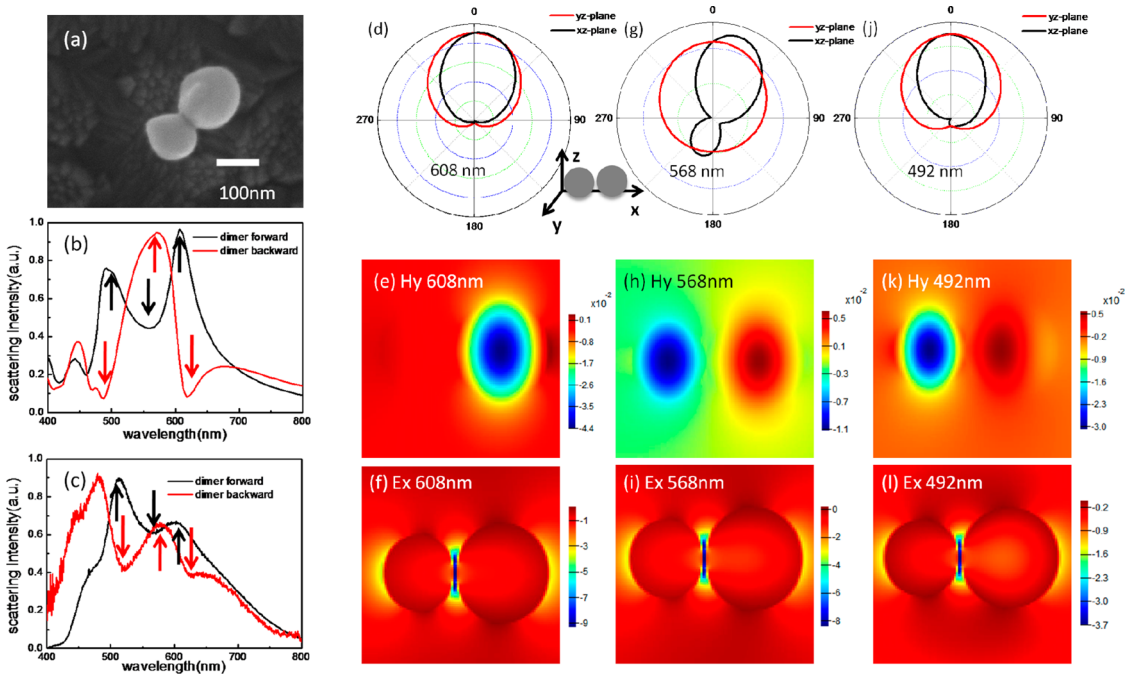

Figure 7. Analysis on the directional scattering properties of a typical heterodimer. (a) The SEM image of a heterodimer with 146.0 and 112.5 nm spheres. (b) The simulated forward (red line) and backward (black line) scattering spectra. The black and red arrows show the correspondence between peaks and dips in back or forward directions. (c) The measured forward (red line) and backward (black line) scattering spectra. Similarly, the black and red arrows show the correspondence between peaks and dips in back or forward directions. (d) Scattering patterns at 608 nm where a Fano resonance dip arises in the backward scattering spectrum, and the scattering direction is almost forward. (e,f) The magnetic field and electric field distributions at 608 nm. (g) Scattering patterns at 568 nm, and the backward scattering intensity reaches the maximum. (h,i) The magnetic field and electric field distributions at 568 nm. (j) Scattering patterns at 492 nm, the second resonance dip in backward direction. (k,l) The magnetic field and electric field distributions at 492 nm. The electric field in the gap possess field enhancement more than 3 times in a broad spectrum region from 608 to 492 nm (f,i,l).

dipole resonance in a single sphere and the electric gap mode in a dimer structure, so the scattering intensity at the electric resonance wavelength in Figure 6f is weakened, and the Fano scattering behavior from a heterodimer (Figure 6g) is similar to the heterodimer with a large gap distance (Figure 4c). Besides increasing the gap distance, the presence of the silica layer changes the refractive index of the sphere relative to the ambient medium and hence influences the Mie coefficients. This may provide another explanation for the differences between experiment and simulation in Figure 2e and h; that is, the gap distance and oxide layer lead to an enhanced back scattering peak near $\lambda = 480$ nm. Moreover, the simulation result in Figure 6h indicates how surface roughness affects the scattering spectra. The scattering spectrum of a 120 nm sphere with about 20 small protuberant hemispheres of diameter 10−20 nm adhering to it is quite similar to the spectrum of a smooth sphere. This is because the dominant magnetic mode of a silicon sphere is inside the sphere (see Figure 3f); surface roughness thus has less of an effect on scattering properties. This is an advantage compared with plasmonic materials for which the resonant mode is on the surface.

The ITO substrates used in our experiment also have some effect on the scattering properties leading to deviations between experiment and simulation. First, the ITO substrate creates image dipoles,[42] which mainly influence the electric gap mode and change the electromagnetic interaction to some extent (Figure S3, Supporting Information). The Fano dip is slightly blue-shifted and the scattering intensities contributed by the quadrupole modes ($\lambda < 400$ nm) are enhanced. Second, the reflection and refraction that happen on the interface, as described by the Fresnel coefficients, also influence the measured scattering spectra. Fortunately, these effects have little influence on the directional scattering behavior.

To better understand the coupling mechanism between electric gap mode and magnetic dipole mode, the electric and magnetic field distributions simulated by FDTD method provides visually and directly the interaction between the electric and magnetic dipole resonances. We choose a typical heterodimer (112.5 and 146.0 nm in Figure 7a) as an example; its forward and backward scattering spectra confirm the analysis of directional Fano resonance in heterodimer above. From simulated spectra in Figure 7b, the two Fano resonance dips at 608 and 492 nm correspond to two peaks in the forward direction, whereas the peak in the backward direction at 568 nm corresponds to the valley in the forward direction. The directional scattering was also verified by experiment (Figure 7c). Some deviation appears caused by measurement differences

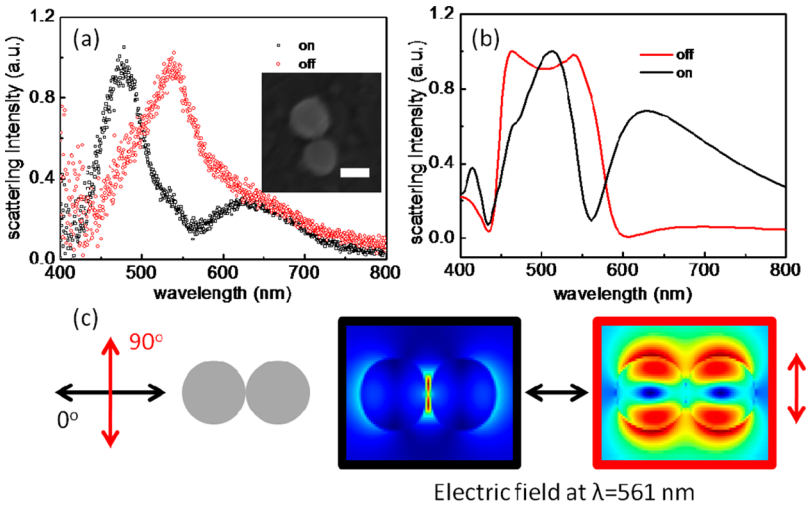

Figure 8. Backward scattering properties under the incident illumination with different polarization direction. (a) The measured scattering spectra under the excitation polarization along the dimer axis (black curve) and normal to the dimer axis (red curve). The inset is the SEM image of this homodimer, and the scale bar is 100 nm. (b) The simulated scattering spectra under the excitation polarization along the dimer axis (black curve) and normal to the dimer axis (red curve). (c) The electric field distributions under different polarization direction at λ = 561 nm.

between forward and backward scattering. A dark-field objective lens (100×, numerical aperture 0.80) was used to illuminate the dimers and collect the scattered light in backward scattering, but in the forward measurement, an oil-immersed dark-field condenser with numerical aperture of 1.4 was used for illumination from beneath the dimers and a dark-field objective lens (100×, numerical aperture 0.80) was used to record the spectra from above. The numerical apertures may have some influence on the collected spectra.[43]

We then analyzed the characteristic wavelengths. First, at 608 nm, the far-field scattering patterns in XZ and YZ plane are obtained (Figure 7d). The unique scattering characteristics yielded unidirectional scattering channels with high forward-to-backward ratio at 608 nm; this ratio was up to 24 times higher, which is superior than that of a single silicon sphere.[29] The magnetic field distribution (Figure 7e) shows the magnetic dipole of a bigger sphere reaching a maximum along the *y*-axis (normal to the polarization of incident wave) first, while the magnetic dipole of the smaller sphere is still very weak. At the same time, the electric field in the gap is very strong (Figure 7f). Both the electric and the magnetic dipoles are along the negative direction, so they have coupled with each other effectively. According to eq 10, they constructively interfere in forward scattering and destructively interfere in backward scattering. Therefore, a characteristic Fano dip can only be seen in the backward spectrum. However, at 568 nm, the situation is different. In Figure 7h, the magnetic dipole of larger silicon sphere changes its direction. Although the magnetic dipole of the smaller sphere begins to increase along the negative direction, the dipole moment is still small. The two magnetic dipoles cancel each other out and reduce $\tilde{\alpha}_{mx}$ in eq 10, while the electric dipole remains strong along the negative direction (Figure 7i). As a result, the forward scattering is weakened whereas the backward scattering is enhanced (Figure 7g). At 492 nm, the positive direction magnetic dipole of 146.0 nm sphere the decreases gradually and the negative-direction magnetic dipole of the 112.5 nm sphere reaches maximum and becomes dominant (Figure 7k). Therefore, the scattering characteristics are similar to that at 608 nm; that is, $\tilde{\alpha}_{mx}$ and $\tilde{\alpha}_{ey}$ have the same sign and are nearly of the same magnitude. They constructively interfere in the forward direction and destructively interfere in the backward direction (Figure 7j). From Figure 7f,i,l, the field distribution just varies slightly, thus verifying that the electric gap mode is quite broad. However, the magnetic resonance is fairly narrow, as seen in Figure 7e,h,k. The magnetization intensity attains maxima at 608 and 492 nm, but decreases and changes direction rapidly. These features are useful in the design and fabrication of nanophotonic devices such as unidirectional nanoantennas and nanosensors.

In our experiments, unpolarized incident light was used to obtain strong scattering signals and reduce noise. The subsequent results are consistent with those from simulations using linear polarized incidence along the dimer axis. Although, if the polarization direction is changed, the scattering spectrum changes significantly because of the absence of the electric gap mode. In Figure 8a, the backward scattering from a homodimer under excitations polarized along the dimer axis is compared with the scattering spectrum under excitations polarized normal to the dimer axis. The polarization direction can operate as an optical switch; the directional Fano resonance is on/off if the polarization is parallel/normal to the dimer axis. The results of simulations (Figure 8b) are similar to those of

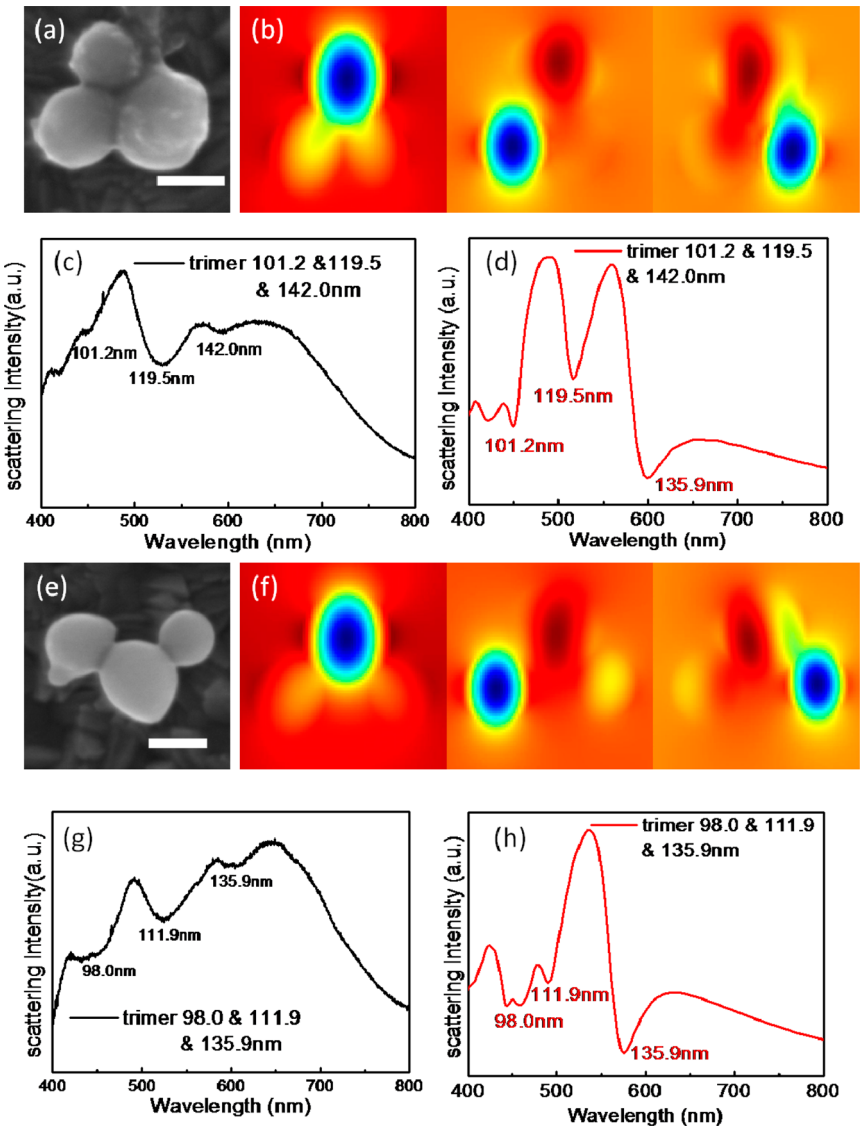

Figure 9. Backward scattering properties of two kinds of silicon nanosphere trimer. (a) SEM image of one trimer, and three spheres with different sizes form a triangle shape. The scale bar is 100 nm. (b) The magnetic field distributions at resonance dips (left to right: 606, 522, and 470 nm). (c) Experimental backward scattering spectrum, and three Fano dips caused by three different spheres are marked with particle sizes. (d) The simulated scattering spectrum, and three resonance dips also can be seen. (e) SEM image of the other trimer in which three spheres form a rectangular triangle shape. (f) The magnetic field distributions at resonance dips (left to right: 585, 501, and 470 nm). (g) The measured scattering spectrum, and three resonance dips can be seen. (h) The simulated scattering spectrum, and three resonance dips are located at 585, 501 and 470 nm.

experiment, although a slight discrepancy is caused by the presence of a gap distance (see inset of Figure 8a). Under excitations polarized normal to the dimer axis, the electric dipole in the silicon spheres no longer couple with each other effectively and cannot generate strong enhancement in the gap (Figure 8c). Hence, the scattering spectrum is similar to that from a single silicon sphere (Figure 8b) when the Fano resonance is turned off by changing the polarization.

In addition, the Fano resonance in silicon trimers is also demonstrated to verify our proposed mechanism. As shown in Figure 9, a silicon nanosphere trimer can generate three Fano resonance dips if the size of each sphere is different. Figure 9a gives a SEM image of a close-packed trimer with 101.2, 119.5, and 142.0 nm-diameter spheres. The measured spectrum (Figure 9c) and calculated spectrum (Figure 9d) both have three Fano dips, and the resonant wavelengths from the experiment are consistent with those from simulations. Considering the broadness of the electric gap mode, the magnetic dipole variation (Figure 9b) is enough to explain the unique spectra. The strong magnetic dipole resonances in each silicon spheres interact with the electric dipole separately causing destructive interference to occur three times at 606, 522, and 470 nm. The change in the aggregate state of silicon trimers does not modify the Fano scattering property. The SEM image of the right triangle shape trimer is shown in Figure 9e. Three Fano dips can be seen in the measured scattering spectrum and

simulated spectrum, and the Fano dips are distinguished by their wavelength 98.0, 111.9, and 135.9 nm to indicate which spheres produce destructive interference (Figure 9g and h). In Figure 9f, the three spheres reach their maximum magnetic response at 585, 501, and 470 nm. Using the conclusion obtained above, we can explain why the scattering spectra, Figure 9g and h, are slightly different. First, the silicon spheres in Figure 9e are not very spherical and have some protrusions, and these may influence the resonance wavelength and strength of the magnetic modes. Second, increasing the vortex angle will decrease the interaction among the three spheres and make the electric gap mode, which is sensitive to the contacting area, spread to the detached two junctions. Hence, the electric gap mode in the experiment may be different from that in the simulation. Third, because the trimer structures have different axes for each pair of spheres, the linear polarized incidence light aligning along the *Y*-axis may not correspond well with that of the experiment. Nonetheless, these differences have little effect on our analysis of the Fano resonance in silicon trimers. By that analogy, engineering the Fano resonances is easily achieved by changing the size or number of silicon nanospheres, and the Fano effect occurs where a silicon sphere reaches its maximum magnetic response.

CONCLUSION

In conclusion, we have presented the first experimental demonstration of the directional Fano resonances in self-assembly silicon nanosphere homodimers, heterodimers, and arbitrary trimers. In comparisons with the numerical simulation and theoretical calculation, we uncovered the coupling mechanism and determined how the electric gap mode and hybrid magnetic mode are generated. The gap between the two spheres can support a broad electric resonance that overlaps with the strong magnetic resonance inside the silicon spheres to produce Fano resonance. The new electric dipole mode and magnetic dipole mode interfere with each other and give rise to enhanced forward scattering and suppressed backward scattering. This Fano resonance is sensitive to gap width and particle size, so we can easily adjust the resonance wavelengths by changing particle size or increasing the number of spheres. Compared with metallic dimers, the absorption loss from the silicon dimers is much lower and the energy is almost radiated in the far field. Moreover, this Fano scattering is sensitive to directional and polarization, which provides promising applications in areas such as unidirectional radiating antennae and polarization-based optical switches.

METHODS

Materials Preparation and Characterization. Silicon nanospheres with diameters from 80 to 200 nm were fabricated by fs-LAL The ultrafast laser has a pulse duration of 35 fs, and a single-pulse energy of 4 mJ. After 10 min of focused laser ablation in deionized water, we were able to suspend the silicon colloid in solution. We then transferred one drop of the solution onto a slab of ITO glass that had been cleaned with acetone, ethanol, and deionized water to remove any pollutant prior to use. During evaporation, the larger droplets split into smaller droplets containing less numbers of silicon spheres. On drying, multiple silicon spheres self-assemble as dimers, trimers or other oligomers *via* capillary forces. Finally, samples were analyzed using a dark-field microscope and a SEM (JSM-7600F) field emission scanning electron microscope operated at 15 kV). To study the surface morphology we used a TEM equipped with a scanning mode (G2 F30, FEI Tecnai, Japan) with an accelerating voltage of 300 kV.

Dark-Field Scattering Measurement. The backward and forward scattering spectra of an individual dimer or trimer were obtained using a dark-field optical microscope (BX51, Olympus) integrated with a quartz-tungsten-halogen lamp (100 W), a monochromator (SpectraPro 2300i, Acton), and a CCD camera (Pixis 400BR_eXcelon, Princeton Instruments). During the measurements the camera was thermoelectrically cooled to −70 °C. The forward and backward scattering measurements are slightly different. In the backward scattering measurement, a dark-field objective lens (100×, numerical aperture 0.80) was used to illuminate the silicon nanospheres with white excitation light. For the forward scattering measurement, an oil immersed dark-field condenser with numerical aperture of 1.4 was used to illuminate the silicon spheres from below. For both, the scattered light was collected by a dark-field objective lens (100×, numerical aperture 0.80). The scattering spectra from the single nanostructures were corrected by first subtracting the background spectra taken from adjacent regions without spheres and then dividing each by the calibrated response curve of the entire optical system. This process ensures both backward and forward scattering spectra can be compared.

Numerical Calculation. The scattering spectra, near-field distributions, and far-field scattering patterns were calculated using the finite-difference time-domain method (FDTD Solutions 8.6.0, Lumerical Solutions, Inc.). The oligomer nanostructures were illuminated with p-polarized plane-wave normal incident visible light (300−900 nm). Linear polarization incidence simplifies the analysis of the near-field distributions and the results well matched those from the unpolarized incident light experiments. A mesh size of 2 nm for the illuminated region was used. Perfectly matched layers were used at the boundary to absorb the directional scattered radiation. The dielectric function of silicon was obtained from Palik.[36] The diameters of silicon spheres were set according to the experimental measurement from SEM images. In the simulations, we calculated the spectra in free space and ignored the ITO substrate because this has little effect on backward scattering spectra.

Conflict of Interest: The authors declare no competing financial interest.

Acknowledgment. The National Basic Research Program of China (2014CB931700) and State Key Laboratory of Optoelectronic Materials and Technologies supported this work.

Supporting Information Available: The changes of electric dipole and magnetic dipole, the scattering cross sections of gold nanosphere and silicon nanosphere both with the diameter of 130 nm, the backward scattering spectra of a heterodimer after considering the ITO substrate. This material is available free of charge *via* the Internet at http://pubs.acs.org.

REFERENCES AND NOTES

1. Miroshnichenko, A. E.; Flach, S.; Kivshar, Y. S. Fano Resonances in Nanoscale Structures. *Rev. Mod. Phys.* **2010**, *82*, 2257–2298.

2. Luk'yanchuk, B.; Zheludev, N. I.; Maier, S. A.; Halas, N. J.; Nordlander, P.; Giessen, H.; Chong, C. T. The Fano Resonance in Plasmonic Nanostructures and Metamaterials. *Nat. Mater.* **2010**, *9*, 707–715.
3. Shafiei, F.; Monticone, F.; Le, K. Q.; Liu, X. X.; Hartsfield, T.; Alu, A.; Li, X. A Subwavelength Plasmonic Metamolecule Exhibiting Magnetic-based Optical Fano Resonance. *Nat. Nanotechnol.* **2013**, *8*, 95–99.
4. Nazir, A.; Panaro, S.; Zaccaria, R. P.; Liberale, C.; Angelis, F. D.; Toma, A. Fano Coil-Type Resonance for Magnetic Hot-Spot Generation. *Nano Lett.* **2014**, *14*, 3166–3171.
5. Hentschel, M.; Saliba, M.; Vogelgesang, R.; Giessen, H.; Alivisatos, A. P.; Liu, N. Transition from Isolated to Collective Modes in Plasmonic Oligomers. *Nano Lett.* **2010**, *10*, 2721–2726.
6. Hao, F.; Sonnefraud, Y.; Dorpe, P. V.; Maier, S. A.; Halas, N. J.; Nordlander, P. Symmetry Breaking in Plasmonic Nanocavities: Subradiant LSPR Sensing and a Tunable Fano Resonance. *Nano Lett.* **2008**, *8*, 3983–3988.
7. Liu, N.; Weiss, T.; Mesch, M.; Langguth, L.; Eigenthaler, U.; Hirscher, M.; Sönnichsen, C.; Giessen, H. Planar Metamaterial Analogue of Electromagnetically Induced Transparency for Plasmonic Sensing. *Nano Lett.* **2010**, *10*, 1103–1107.
8. Wu, C.; Khanikaev, A. B.; Adato, R.; Arju, N.; Yanik, A. A.; Altug, H.; Shvets, G. Fano-Resonant Asymmetric Metamaterials for Ultrasensitive Spectroscopy and Identification of Molecular Monolayers. *Nat. Mater.* **2012**, *11*, 69–75.
9. Chang, W. S.; Lassiter, J. B.; Swanglap, P.; Sobhani, H.; Khatua, S.; Nordlander, P.; Halas, N. J.; Link, S. A Plasmonic Fano Switch. *Nano Lett.* **2012**, *12*, 4977–4982.
10. Vercruysse, D.; Sonnefraud, Y.; Verellen, N.; Fuchs, F. B.; Martino, G. D.; Lagae, L.; Moshchalkov, V. V.; Maier, S. A.; Dorpe, P. V. Unidirectional Side Scattering of Light by a Single-Element Nanoantenna. *Nano Lett.* **2013**, *13*, 3843–3849.
11. Lassiter, J. B.; Sobhani, H.; Knight, M. W.; Mielczarek, W. S.; Nordlander, P.; Halas, N. J. Designing and Deconstructing the Fano Lineshape in Plasmonic Nanoclusters. *Nano Lett.* **2012**, *12*, 1058–1062.
12. Fan, J. A.; Bao, K.; Wu, C.; Bao, J.; Bardhan, R.; Halas, N. J.; Manoharan, V. N.; Shvets, G.; Nordlander, P.; Capasso, F. Fano-like Interference in Self-Assembled Plasmonic Quadrumer Clusters. *Nano Lett.* **2010**, *10*, 4680–4685.
13. Fan, J. A.; Wu, C.; Bao, K.; Bao, J.; Bardhan, R.; Halas, N. J.; Manoharan, V. N.; Nordlander, P.; Shvets, G.; Capasso, F. Self-Assembled Plasmonic Nanoparticle Clusters. *Science* **2010**, *328*, 1135–1138.
14. Hao, F.; Nordlander, P.; Sonnefraud, Y.; Van Dorpe, P.; Maier, S. A. Tunability of Subradiant Dipolar and Fano-Type Plasmon Resonances in Metallic Ring/Disk Cavities: Implications for Nanoscale Optical Sensing. *ACS Nano* **2009**, *3*, 643–652.
15. Lovera, A.; Gallinet, B.; Nordlander, P.; J. F. Martin, O. Mechanisms of Fano Resonances in Coupled Plasmonic Systems. *ACS Nano* **2013**, *7*, 4527–4536.
16. Artar, A.; Yanik, A. A.; Altug, H. Directional Double Fano Resonances in Plasmonic Hetero-Oligomers. *Nano Lett.* **2011**, *11*, 3694–3700.
17. Biswas, S.; Duan, J.; Nepal, D.; Park, K.; Pachter, R.; Vaia, R. A. Plasmon-Induced Transparency in the Visible Region *via* Self-Assembled Gold Nanorod Heterodimers. *Nano Lett.* **2013**, *13*, 6287–6291.
18. Woo, K. C.; Shao, L.; Chen, H.; Liang, Y.; Wang, J.; Lin, H. Q. Universal Scaling and Fano Resonance in the Plasmon Coupling between Gold Nanorods. *ACS Nano* **2011**, *5*, 5976–5986.
19. Brown, L. V.; Sobhani, H.; Lassiter, J. B.; Nordlander, P.; Halas, N. J. Heterodimers: Plasmonic Properties of Mismatched Nanoparticle Pairs. *ACS Nano* **2010**, *4*, 819–832.
20. Bachelier, G.; Russier-Antoine, I.; Benichou, E.; Jonin, C.; Del Fatti, N.; Vallée, F.; Brevet, P. F. Fano Profiles Induced by Near-Field Coupling in Heterogeneous Dimers of Gold and Silver Nanoparticles. *Phys. Rev. Lett.* **2008**, *101*, 197401.
21. Miroshnichenko, A. E.; Kivshar, Y. S. Fano Resonances in All-Dielectric Oligomers. *Nano Lett.* **2012**, *12*, 6459–6463.
22. Chong, K. E.; Hopkins, B.; Staude, I.; Miroshnichenko, A. E.; Dominguez, J.; Decker, M.; Neshev, D. N.; Brener, I.; Kivshar, Y. S. Observation of Fano Resonances in All-Dielectric Nanoparticle Oligomers. *Small* **2014**, *10*, 1985–1990.
23. Rybin, M. V.; Khanikaev, A. B.; Inoue, M.; Samusev, K. B.; Steel, M. J.; Yushin, G.; Limonov, M. F. Fano Resonance between Mie and Bragg Scattering in Photonic Crystals. *Phys. Rev. Lett.* **2009**, *103*, 023901.
24. Ashili, S. P.; Astratov, V. N. The Effects of Inter-Cavity Separation on Optical Coupling in Dielectric Bispheres. *Opt. Express* **2006**, *14*, 9460–9466.
25. Rybin, M. V.; Kapitanova, P. V.; Filonov, D. S.; Slobozhanyuk, A. P.; Belov, P. A.; Kivshar, Y. S.; Limonov, M. F. Fano Resonances in Antennas: General Control over Radiation Patterns. *Phys. Rev. B: Condens. Matter Mater. Phys.* **2013**, *88*, 205106.
26. Hopkins, B.; Poddubny, A. N.; Miroshnichenko, A. E.; Kivshar, Y. S. Revisiting the Physics of Fano Resonances for Nanoparticle Oligomers. *Phys. Rev. A: At., Mol., Opt. Phys.* **2013**, *88*, 053819.
27. Evlyukhin, A. B.; Novikov, S. M.; Zywietz, U.; Eriksen, R. L.; Reinhardt, C.; Bozhevolnyi, S. I.; Chichkov, B. N. Demonstration of Magnetic Dipole Resonances of Dielectric Nanospheres in the Visible Region. *Nano Lett.* **2012**, *12*, 3749–3755.
28. Kuznetsov, A. I.; Miroshnichenko, A. E.; Fu, Y. H.; Zhang, J. B.; Luk'yanchuk, B. Magnetic Light. *Sci. Rep.* **2012**, *2*, 492.
29. Fu, Y. H.; Kuznetsov, A. I.; Miroshnichenko, A. E.; Yu, Y. F.; Luk'yanchuk, B. Directional Visible Light Scattering by Silicon Nanoparticles. *Nat. Commun.* **2013**, *4*, 1527.
30. Shalaev, V. M. Optical Negative-Index Metamaterials. *Nat. Photonics* **2007**, *1*, 41–48.
31. Albella, P.; Poyli, M. A.; Schmidt, M. K.; Maier, S. A.; Moreno, F.; Saenz, J. J.; Aizpurua, J. Low-Loss Electric and Magnetic Field-Enhanced Spectroscopy with Subwavelength Silicon Dimers. *J. Phys. Chem. C* **2013**, *117*, 13573–13584.
32. Kerker, M.; Wang, D. S.; Giles, C. L. Electromagnetic Scattering by Magnetic Spheres. *J. Opt. Soc. Am.* **1983**, *73*, 765–767.
33. Garcia-Camara, B.; Saiz, J. M.; Gonzalez, F.; Moreno, F. Nanoparticles with Unconventional Scattering Properties: Size Effects. *Opt. Commun.* **2010**, *283*, 490–496.
34. Person, S.; Jain, M.; Lapin, Z.; Saenz, J. J.; Wicks, G.; Novotny, L. Demonstration of Zero Optical Backscattering from Single Nanoparticles. *Nano Lett.* **2013**, *13*, 1806–1809.
35. Shegai, T.; Chen, S.; Miljkovic, V. D.; Zengin, G.; Johansson, P.; Käll, M. A Bimetallic Nanoantenna for Directional Colour Routing. *Nat. Commun.* **2011**, *2*, 481.
36. Palik, E. D. *Handbook of Optical Constants of Solids*; Academic Press: New York, 1998; Vol. 3.
37. Zhang, W.; Gallinet, B.; Martin, O. J. F. Symmetry and Selection Rules for Localized Surface Plasmon Resonances in Nanostructures. *Phys. Rev. B: Condens. Matter Mater. Phys.* **2010**, *81*, 233407.
38. Krasnok, A. E.; Simovski, C. R.; Belov, P. A.; Kivshar, Y. S. Superdirective Dielectric Nanoantennas. *Nanoscale* **2014**, *6*, 7354–7361.
39. Prodan, E.; Radloff, C.; Halas, N. J.; Nordlander, P. A Hybridization Model for the Plasmon Response of Complex Nanostructures. *Science* **2003**, *302*, 419–422.
40. Bohren, C. F.; Huffman, D. R. *Absorption and Scattering of Light by Small Particles*; Wiley-Interscience: New York, 1983.
41. Liu, W.; Miroshnichenko, A. E.; Neshev, D. N.; Kivshar, Y. S. Broadband Unidirectional Scattering by Magneto-Electric Core Shell Nanoparticles. *ACS Nano* **2012**, *6*, 5489–5497.
42. Gay-Balmaz, P.; Martin, O. J. F. Validity Domain and Limitation of Non-retarded Green's Tensor for Electromagnetic Scattering at Surfaces. *Opt. Commun.* **2000**, *184*, 37–47.
43. Knight, M. W.; Fan, J.; Capasso, F.; Halas, N. J. Influence of Excitation and Collection Geometry on the Dark Field Spectra of Individual Plasmonic Nanostructures. *Opt. Express* **2010**, *18*, 2579–2587.